4*d*-inner-shell ionization of Xe^+ ions and subsequent Auger decay

M. A. Khalal,[1] P. Lablanquie,[1] L. Andric,[1,2] J. Palaudoux,[1] F. Penent,[1] K. Bučar,[3] M. Žitnik,[3] R. Püttner,[4] K. Jänkälä,[5] D. Cubaynes,[6,7] S. Guilbaud,[6,7] and J.-M. Bizau[6,7]

[1]*Sorbonne Université, UPMC Université Paris 06, Centre National de la Recherche Scientifique, LCP-MR (UMR 7614), 4 place Jussieu, 75252 Paris Cedex 05, France*

[2]*Université Paris-Est, 5 boulevard Descartes, F-77454 Marne-la Vallée Cedex 2, France*

[3]*Jozef Stefan Institute, Jamova cesta 39, SI-1001 Ljubljana, Slovenia*

[4]*Fachbereich Physik, Freie Universität Berlin, Arnimallee 14, D-14195 Berlin, Germany*

[5]*Nano and Molecular Systems Research Unit, University of Oulu, P.O. Box 3000, 90014 Oulu, Finland*

[6]*ISMO, Centre National de la Recherche Scientifique UMR 8214, Université Paris-Sud, Université Paris-Saclay, 91405 Orsay, France*

[7]*Synchrotron SOLEIL, l'Orme des Merisiers, Saint-Aubin, Boîte Postale 48, 91192 Gif-sur-Yvette Cedex, France*

(Received 17 May 2017; published 14 July 2017)

We have studied Xe^+4d inner-shell photoionization in a direct experiment on Xe^+ ions, merging an ion and a photon beam and detecting the ejected electrons with a cylindrical mirror analyzer. The measured 4*d* photoelectron spectrum is compared to the 4*d* core valence double ionization spectrum of the neutral Xe atom, obtained with a magnetic bottle spectrometer. This multicoincidence experiment gives access to the spectroscopy of the individual $Xe^{2+}\ 4d^{-1}\,5p^{-1}$ states and to their respective Auger decays, which are found to present a strong selectivity. The experimental results are interpreted with the help of *ab initio* calculations.

DOI: 10.1103/PhysRevA.96.013412

I. INTRODUCTION

Direct photoelectron spectroscopy experiments on ions are extremely difficult due to the relatively low target ion density in the source volume of an electron spectrometer, and also because of the high cross section for ionizing collision of ions on the background gas: photoionization of this background gas (even in ultra-high-vacuum conditions) produces a high background electron signal. Therefore direct electron spectroscopic experiments on ions have been reported only in a few cases in the 1990's, such as the resonant Auger decay of Ca^+ ions [1–3] or the 4*d* photoionization of Xe^+ ions [4]. Recently, the field has regained interest thanks to the development of powerful synchrotron radiation sources and to the use of a second generation of dedicated experiments such as the MAIA setup installed on the PLEIADES beam line at the synchrotron radiation facility SOLEIL [5]. As an example, this setup enabled the detailed study of the Auger decay of the $4d \rightarrow nf$ ($n = 4, 5$) resonances in the Xe^{5+} ion [6]. Here we present another example of these experimental studies of ions and revisit the 4*d* inner-shell ionization of the Xe^+ ions first reported by Gottwald *et al.* in 1999 [4].

In addition, we use a complementary experimental approach for this paper, namely, core valence double ionization of the neutral xenon atoms. The high efficiency of multiple coincidence experiments with a magnetic bottle allows one to observe in detail these core valence double ionization paths as demonstrated by Hikosaka *et al.* in 2006 on Ne and N_2 targets [7]. It was later shown that this approach can be applied to infer properties of the inner-shell ionization of atomic ions, with Ar^+ as an example [8]. The targets Hg^+ [9,10] and Kr^+ [11] were recently addressed. We show here that the present core valence results on Xe atoms validate the experimental results obtained using the MAIA setup on 4*d* shell ionization of Xe^+ ions. Furthermore coincidence filtering of data collected by the magnetic bottle gives access to the Auger decay of each selected $Xe^{2+}\ 4d^{-1}\,5p^{-1}$ state.

Below we report a spectroscopic study of the Xe^{2+*} states resulting from photoionization of a 4*d* shell in the Xe^+ ion, and present the corresponding state resolved Auger decay. Calculations of transition energies and decay rates have been performed to guide and support the interpretation of the experimental results.

II. EXPERIMENTS

A. MAIA experiment

The experiment on the Xe^+ ion was performed with the MAIA merged-beam setup on the PLEIADES beam line of the synchrotron radiation facility SOLEIL [5,6]. The ions are produced in a 12.4-GHz permanent magnet electron cyclotron resonance ion source (ECRIS) by heating ^{129}Xe isotopic gas. They are accelerated to 4 keV and selected using a dipole magnet. The Xe^+ ions are then focused and merged with the photon beam into the source volume of a cylindrical mirror electron analyzer (CMA) [12]. Both ion and photon beams are collinear to the CMA axis. Typical currents of focused ions were 2 μA. A second dipole magnet separates the incident Xe^+ ions from the Xe^{q+} ($q = 2, 3$) ions produced in the photoionization processes, which are counted by the microchannel plate detector. The photoelectrons emitted at the magic angle in the laboratory frame are counted as a function of their kinetic energy by eight channeltron detectors placed at the CMA focal plane. In order to reduce the strong background in the electron signal produced by collisional processes between the fast Xe^+ beam and the residual gas in the CMA chamber or the metallic surfaces, and to suppress the signal resulting from photoionization of neutral Xe coming from the ECR source, the photoelectrons are detected in coincidence with the photoions (PEPICO = Photo Electron Photo Ion Coincidence) [4,6]. To improve the ratio of true-to-false coincidences further, a 150-V negative bias was applied to a 20-cm-long region centered at the source volume of the CMA. The photoions produced

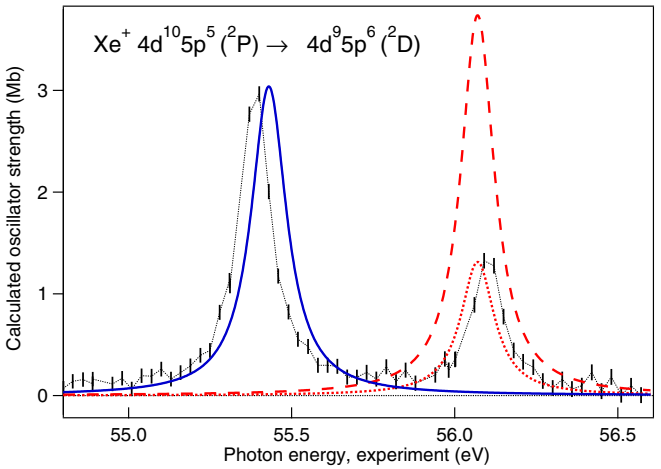

FIG. 1. Experiment with MAIA setup on Xe^+ ions: Xe^{2+} ion yield recorded in the region of the $4d \rightarrow 5p$ resonances with 20-meV bandpass. The vertical error bars represent the statistical uncertainty. The resonance at lower energy corresponds to the $^2P_{3/2} \rightarrow {}^2D_{5/2}$ transition and the higher one corresponds to the $^2P_{1/2} \rightarrow {}^2D_{3/2}$ transition. The photon energy scale has been calibrated using data from Ref. [14]. Experimental results are scaled to the calculated cross section of the lower-lying resonance (blue solid line); adjustment of the calculated cross section for the second resonance (red dashed curve) with the experiment values (red dotted curve) gives the proportion of Xe^+ ions in the ground ($^2P_{3/2}$) and metastable ($^2P_{1/2}$) states, which is found to be 74 and 26%. See text for details. Note that the theoretical curves have been shifted by +150 meV to match better the positions of the resonances.

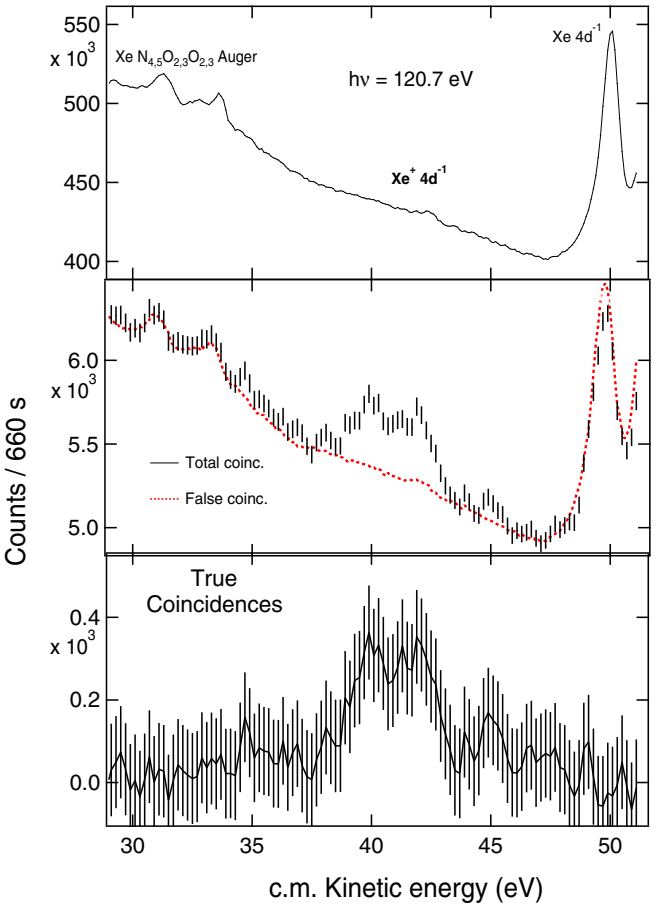

FIG. 2. Experiment with MAIA setup on Xe^+ ions. Top: Raw photoelectron spectrum, represented as a function of the center-of-mass kinetic energy. Middle: Photoelectron spectrum in coincidence with Xe^{3+} ions (points with error bars). The red (dotted) curve gives the estimated false coincidence spectrum (see text for details). The bottom curve represents the resulting true coincidence spectrum (line with error bars). The photon energy was 120.7 eV and the spectral bandpass was 110 meV. The error bars give the statistical uncertainty.

inside this region therefore have different velocity from the ions produced outside and can be discriminated by the second dipole magnet.

Because the plasma in the ECRIS is quite hot, the Xe^+ ions are produced not only in the ground state $Xe^+ \, 4d^{10} \, 5s^2 \, 5p^5$ ($^2P_{3/2}$), but also in the metastable state $Xe^+ \, 4d^{10} \, 5s^2 \, 5p^5$ ($^2P_{1/2}$). The latter state does not decay before the ions arrive in the interaction region (lifetime 49 ms [13]) and thus contributes to our photoelectron spectra. To estimate relative populations of the ions in the two levels, we have measured the yield of Xe^{2+} photoions in the energy region of the $Xe^+ \, 4d^{10} \, 5s^2 \, 5p^5 \, (^2P_{Ji}) \rightarrow Xe^+ \, 4d^9 \, 5s^2 \, 5p^6 \, (^2D_{Jf})$ photoexcitations. The result is shown in Fig. 1. The strongest resonance at 55.4 eV corresponds to the transition $J_i = 3/2 \rightarrow J_f = 5/2$ [14] of ions in the ground state, and the one at 56.1 eV corresponds to the transition $J_i = 1/2 \rightarrow J_f = 3/2$ of ions in the metastable state. Figure 1 also displays the calculated results for the corresponding transitions (see Sec. III). For the resonance lower in energy we obtain an oscillator strength of 0.1336 and for that higher in energy we obtain a value of 0.1660. The calculated position and natural linewidth are 55.28 eV and 132 meV for the lower and 55.92 eV and 125 meV for the upper resonance, in quite good agreement with experimental values from the literature reporting 55.39 and 56.08 eV for the energy positions [14], and 111 ± 3 and 104 ± 3 meV for the widths [15], respectively. A comparison of the measured intensities of these two well-separated resonances with the calculated oscillator strengths allows us to estimate the initial populations: by assuming that the calculated oscillator strengths are correct one obtains that the observed intensity ratio equals the ratio of calculated oscillator strengths multiplied by the population ratio. The best description of the experimental spectrum is obtained taking 74% of the ions in the ground level and 26% in the excited level, which is close to the statistical population ratio (66% for $^2P_{3/2}$ and 33% for $^2P_{1/2}$).

Figure 2 shows the electron spectra recorded at 120.7 eV photon energy. This energy was chosen to avoid any overlap between the $4d^{-1}$ photoelectron and Auger lines. The top panel displays the total electron spectrum as a function of electron kinetic energy. The spectrum is dominated by a high and decreasing background produced by the collisions of the beam of Xe^+ ions with residual gas (mainly Xe and H_2). The most intense lines can be identified as resulting from $4d$ photoionization of neutral xenon. The strongest line at 50 eV corresponds to the Xe $4d_{3/2}^{-1}$ photoelectrons and the less intense lines below 35 eV correspond to the $N_{4,5}OO$ Auger electrons. One possible reason for the presence of these lines is the

drifting of neutral Xe from the ion source. The pressure in the CMA chamber was 8×10^{-9} mbar. These spurious lines are, however, useful for determination of the precise photon energy and for the calibration of the CMA energy scale. They allow us to quantify electron energy shifts induced by the contact and plasma potentials and to extract the electron kinetic energy in the laboratory frame. A further correction due to the Doppler effect is applied to obtain electron kinetic energy in the frame of the Xe^+ ions which is used to present the spectra in Fig. 2.

The weak photoelectron lines produced in the photoionization in the 4d subshell of the Xe^+ ions are separated out by the application of electron-ion coincidence technique. These lines are clearly unveiled in the electron spectrum shown in Fig. 2 middle (black points with statistical error bars) which represents the electron signal recorded in coincidence with the Xe^{3+} photoions. The background and the neutral Xe lines are still present because of the false coincidence events (true/false ratio ~1:10), but their intensity is reduced by two orders of magnitude. The Xe^{3+} ions generated by double Auger decay subsequent to the 4d ionization of neutral Xe are not detected by the present experimental setup since they are not moving with the ion beam. The false coincidence signal can be estimated (red curve) by normalization to the electron signal, because the photoion signal remained constant during the recording of the spectra. Upon subtraction, only the signal due to the Xe^+ ions remains visible (Fig. 2, bottom).

B. High-energy resolution multielectron coincidence spectroscopy experiment

The core + valence double ionization experiment on neutral Xe atoms was performed with the son of MAIA, the high-energy resolution multielectron coincidence spectroscopy (HERMES) experiment, on the SEXTANTS beam line of the synchrotron radiation facility SOLEIL [16]. The HERMES setup has been described previously (see Ref. [17] and references included). Briefly, multielectron coincidences were recorded using a magnetic bottle electron time-of-flight spectrometer of the type developed by Eland *et al.* [18]. The single-bunch operation mode of the synchrotron was used and the electron flight times were measured by a time to digital converter (TDC) with 120-ps discretization step (TDC-V4 developed at the LUMAT federation in Orsay, France). A mechanical chopper was applied to reduce the number of light bunches by a factor of 10, in order to effectively extend the 1184-ns single bunch repetition time to ~12.5 μs [19]. Calibration and conversion from electron time of flight to the electron kinetic energy were based on the Xe 4d Auger electrons the energies of which are precisely known [20]. The energy resolution ΔE for electrons of energy E is found to obey the relation $\Delta E/E = 1.6\%$ for E above 1 eV and is limited to ~20 meV for smaller energies. The core valence double ionization of Xe atoms was investigated at two photon energies (135 and 120 eV). The results presented here were obtained at the lower photon energy after accumulating the spectra for ~5 h. The photon energy resolution was set to 15 meV. In order to diminish false coincidences, the electron count rate was limited to 2 kHz.

III. THEORY

Calculations were performed within the well-established configuration interaction Dirac-Fock framework using the GRASP2K code [21]. In the method one first solves relativistic one-electron wave functions from the Dirac-Fock equations in an average level scheme. Then the final atomic state functions are solved by diagonalizing the Dirac-Coulomb Hamiltonian in a basis of jj-coupled configuration state functions. The final states are thus linear combinations of configuration state functions of the same parity P, total angular momentum J, and its projection M. For further details, see, for example, Refs. [21,22].

The atomic and singly charged ionic states were constructed from Xe $[4d^{10}\,5s^2\,5p^6]$ and $Xe^+[4d^9\,5s^2\,5p^6]$ configurations, respectively. The calculation of Xe^{2+} and Xe^{3+} states included also some excitations to $4f$, $5d$, $6s$, and $6p$ orbitals. The Xe^{2+} states were constructed from odd parity $Xe^{2+}[4d^9\,5s^2\,5p^5,\ 4d^9\,5s^2\,5p^4 4f,\ 4d^9\,5s^2\,5p^4 6p]$ configurations and Xe^{3+} states were constructed from Xe^{3+} $[5s^0\,5p^5,\ 5s5p^4, 5s^2\,5p^3]$ and $Xe^{3+}[5p^4nl,\ 5s5p^3nl,\ 5s^2\,5p^2nl]$, where nl is $4f$, $5d$, $6s$, or $6p$. From the Xe^{2+} states only the lowest 12 states in energy were calculated as they correspond to the measured $Xe^{2+}[4d^9\,5s^2\,5p^5]$ states. For Xe^{3+} the above given configurations yield 411 states from which the lowest 129 are energetically accessible from the 12 Xe^{2+} initial states by the Auger decay. The lifetimes of $Xe^+[4d^9]$ states were obtained from calculated Auger rates to states constructed from the main $Xe^{2+}[5s\,5p]^{-2}$ configurations and the correlating configurations $Xe^{2+}[4f^2\,5s5p^3,\ 4f^2\,5s^0\,5p^4,\ 4f5s5p^4,\ 4f5s^2\,5p^3,\ 4f5s^0\,5p^5,\ 5s^2\,5p^3\,5d,\ 5s^2\,5p^2\,5d^2,\ 5s5p^4\,5d,\ 5s^0\,5p^4\,5d^2]$.

The fluorescence, one-electron photoionization, and Auger decay transition matrix elements were obtained using the reos, photo, and Auger components of the RATIP utility package of GRASP [23], respectively. All dipole matrix elements were calculated in the length gauge. The relative Xe → Xe^{2+} double ionization cross sections were estimated simply by assuming them to be directly proportional to the statistical weights $(2J + 1)$ of the final LS states of the doubly charged ion. The LS coupling coefficients were obtained by transforming the calculated jj-coupled configuration state function coefficients using the LSJ program [24].

IV. RESULTS AND DISCUSSION

A. Results with MAIA experiment on the 4d-inner-shell ionization of Xe^+ ions

Figure 3(b) shows our measurement of the photoelectron spectrum resulting from 4d photoionization of Xe^+ ions:

$$Xe^+ + h\nu \rightarrow Xe^{2+*}(4d^{-1}\,5p^{-1}) + e^-_{\rm ph}. \qquad (1)$$

The data are identical to those in Fig. 2 bottom with the difference that they are here presented on a binding-energy scale relative to the ground state of the Xe^+ ion. Note that for the experiments performed on the neutral species, see below, a binding-energy scale relative to the ground state of the Xe atom is used; these two scales differ by 12.13 eV equal to the $5p$ ionization potential in Xe I. The data are compared with the pioneering measurements published in 1999 by Gottwald *et al.* [Fig. 3(a)] [4]. Large error bars clearly testify the

difficulty of such an experiment. However, we clearly observe a broad unresolved photoelectron peak located in the 78–82-eV binding-energy region. This is in disagreement with Gottwald *et al.* who instead report on three broad structures at 72.2, 74.9, and 76.2 eV, that is, in a region where we do not detect any photoelectron signal within our error bars. The expected energy positions of the $Xe^{2+}\,4d^{-1}\,5p^{-1}$ states which are populated upon $4d$ shell ionization of Xe^{+} $(5p^{-1})$ states can be deduced from the literature, namely, from the measurement by Kivimäki *et al.* [25] of the "$4p$" photoelectron spectrum of the Xe atom and of the associated "N_3" $N_{4,5}O_{2,3}$ Coster-Kronig decay to these $Xe^{2+}\,4d^{-1}\,5p^{-1}$ states. They are summarized in Table I using the binding-energy scale relative to the ground state of the Xe atom. Moreover, they are indicated by vertical bars in Fig. 3, where the broad blue and thin red bars show the expected energy positions for an ionization of the Xe^{+} ion in the ground state $5p^{-1}$ $(^2P_{3/2})$ and the metastable state $5p^{-1}$ $(^2P_{1/2})$, respectively. Clearly, these estimates match our experimental results and not those of Gottwald *et al.*

To confirm this interpretation further, we have calculated the cross section for $4d$ inner-shell photoionization of Xe^{+} ions, both from the $^2P_{3/2}$ ground state and from the $^2P_{1/2}$ excited state. The results of the calculation performed at a photon energy of 120.7 eV are given in Table I. The calculated cross sections are displayed in Fig. 3(c) using the same color convention as for the expected positions (see above): blue shows photoionization from the Xe^{+} ground state $5p^{-1}$ $(^2P_{3/2})$, while red displays photoionization from the Xe^{+} excited state $5p^{-1}$ $(^2P_{1/2})$. The two contributions have been weighted by taking into account the estimated initial populations of ground state and metastable Xe^{+} ions (see Sec. II A). The shape of the peaks is a pure Lorentzian curve, reflecting the calculated lifetime of the individual $Xe^{2+}\,4d^{-1}\,5p^{-1}$ states (see Table I). A convolution with a 700-meV full width at half maximum Gaussian function (in black) is used to simulate experimental resolution; the comparison fully confirms that the broad unresolved structure that we observe at 78–82 eV corresponds to $4d$ photoelectron peaks in the Xe^{+} ion. A closer look at the intensity of the calculated photoelectron peaks (see Fig. 3 and Table I) shows that the photoionization of the Xe^{+} ion in the ground and in the metastable state results in completely different populations of the $Xe^{2+}\,4d^{-1}\,5p^{-1}$ final states. For instance, the population of the Xe^{2+} states at lower binding energy is suppressed when starting from the Xe^{+} metastable state. This effect originates from the selection and propensity rules of the single photoionization process. For instance, if we consider $4d$ photoionization from the metastable Xe^{+} state $5p^{-1}$ $(^2P_{1/2})$, and assume that the $5p_{1/2}^{-1}$ hole remains a spectator, then the resulting Xe^{2+} final states will be in major part composed of $4d_{3/2}^{-1}5p_{1/2}^{-1}$ or $4d_{5/2}^{-1}5p_{1/2}^{-1}$ configuration. The ^SL_j terms generated from these configurations do not include the low-lying $^3F_4$ and $^3P_0$ terms, which explains why these levels are found to have zero intensity in our calculation (see Table I).

A further argument demonstrating the validity of our present measurement of the $4d$ photoelectron spectrum of Xe^{+} ions is given by a comparison with the results of the core valence double ionization of the neutral Xe atom that we present next.

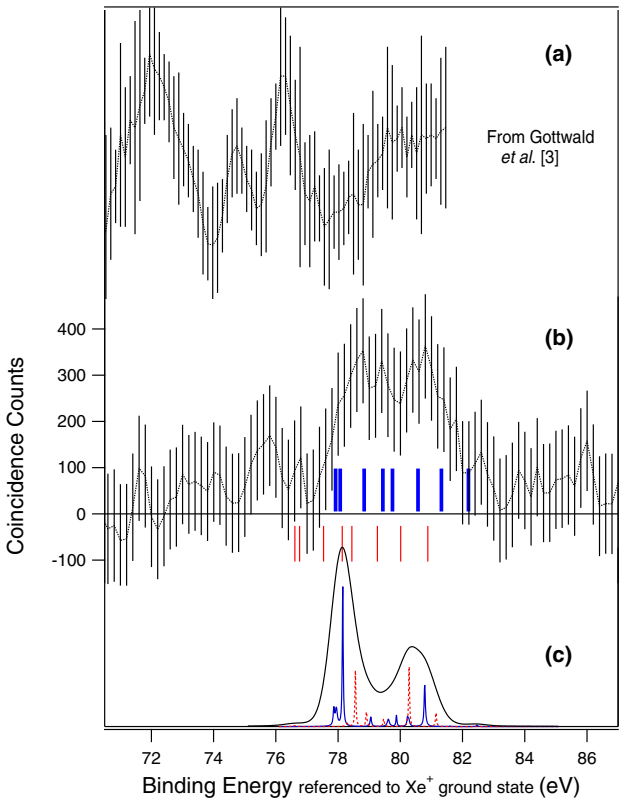

FIG. 3. (b) Experiment with MAIA setup: $4d$ photoelectron spectrum from photoionization of Xe^{+} ions with 120.7 eV photons (middle). It is compared to the previous experiment by Gottwald *et al.* [4] at $h\nu = 103.3$ eV (a, top). The broad blue and thin red vertical bars indicate the expected energy positions for the $Xe^{+}\,5p^{-1}(^2P_{3/2}) \rightarrow Xe^{2+}\,4d^{-1}\,5p^{-1}$ and the $Xe^{+}\,5p^{-1}(^2P_{1/2}) \rightarrow Xe^{2+}\,4d^{-1}\,5p^{-1}$ transitions, respectively; the transition energies are estimated using the $4d^{-1}\,5p^{-1}$ binding energies of Kivimäki *et al.* [25]. The blue (solid) and red (dotted) curves in the bottom graph (c) show the calculated Xe^{+} $(^2P_{3/2}) \rightarrow Xe^{2+}\,4d^{-1}\,5p^{-1}$ and Xe^{+} $(^2P_{1/2}) \rightarrow Xe^{2+}\,4d^{-1}\,5p^{-1}$ photoelectron spectra, respectively. The spectra are weighted according to the estimated Xe^{+} $(^2P_{3/2})$ to Xe^{+} $(^2P_{1/2})$ ratio in the ion beam. The lines are broadened by the Lorentzian lifetime contribution only. The black line shows the calculated spectrum with additional 700 meV Gaussian broadening to simulate the effect of the experimental resolution. Note that theoretical curves have been shifted by +2 eV to match the positions expected from Ref. [25] (vertical bars).

B. Results with HERMES experiment on the core valence double ionization of neutral Xe atoms

1. *Spectroscopy of the* $Xe^{2+}\,4d^{-1}\,5p^{-1}$ *states*

The HERMES experiment was used to study the core valence double photoionization of neutral Xe atoms, and the subsequent Auger decay of these Xe^{2+} intermediate states:

$$Xe + h\nu \rightarrow Xe^{2+*}\,(4d^{-1}\,5p^{-1}) + e^{-}_{ph1} + e^{-}_{ph2} \qquad (2a)$$

$$\rightarrow Xe^{2+*}\,(4d^{-1}\,5p^{-1}) \rightarrow Xe^{3+} + e^{-}_{Auger}. \qquad (2b)$$

This paper is motivated by the fact that the same Xe^{2+*} $(4d^{-1}\,5p^{-1})$ intermediate states are populated here as in the photoionization of Xe^{+} ions [see Eq. (1)]. Although they

TABLE I. Binding energies (with respect to the Xe ground state) and assignments of the Xe^{2+} ($4d^{-1}\,5p^{-1}$) core valence states in both (j,j) J and LSJ coupling ($j_1 = 4d_{j1}^{-1}\, j_2 = 5p_{j2}^{-1}$). The present experimental values (first column) are compared to the $4p$ Auger experiment by Kivimäki *et al.* [25] and to the threshold electron coincidence experiment by Bolognesi *et al.* [29]. The table gives also the calculated lifetime broadening and the cross section for formation by photoionization of a Xe^+ ion.

$4d^{-1}\,5p^{-1}$ Binding energy (relative to Xe ground state)				$4d^{-1}\,5p^{-1}$ Assignment						Lifetime Broadening	Calculated cross section for $4d$ photoionization (hv 120.7 eV)	
				J J coupling		*LS* coupling						
Experiment eV	[25] eV	[29] eV	Theory eV	(j_1,j_2) J	c^2 %	$^{2S+1}L_J$	c_1^2 %	$^{2S+1}L_J$	c_2^2 %	meV	$Xe^{+2}\,P_{3/2}$ Mb	$Xe^{+*\,2}P_{1/2}$ Mb
		90.39	(1) 87.99	(5/2,3/2) 2	91	$^1D_2$	69			48	0.335	0.063
(A) 90.14	90.05	90.67	(2) 88.07	(5/2,3/2) 3	94	$^3D_3$	90			79	0.586	0.067
	90.20	90.86	(3) 88.28	(5/2,3/2) 4	100	$^3F_4$	100			35	2.095	0
(B) 91.00	90.97 $^3D_1$	91.19 $^3D_1$	(4) 89.18	(5/2,3/2) 1	92	$^1P_1$	43	$^3D_1$	32	51	0.213	0.020
	91.57	91.93	(5) 89.74	(3/2,3/2) 2	67	$^3D_2$	87			81	0.256	0.298
(C1) 91.86	91.88	92.30	(6) 90.00	(5/2,1/2) 3	71	$^3F_3$	93			37	0.179	2.506
(C2) 92.17		92.74	(7) 90.36	(5/2,1/2) 2	61	$^3P_2$	78			43	0.130	0.769
			(8) 90.40	(3/2,3/2) 1	89	$^3P_1$	50	$^3D_1$	49	70	0.207	0.030
(D) 92.78	92.70	93.47	(9) 90.91	(3/2,3/2) 3	70	$^1F_3$	87			47	0.820	0.430
		93.12	(10) 90.96	(3/2,3/2) 0	100	$^3P_0$	100			98	0.069	0
(E) 93.60	93.45	94.11	(11) 91.73	(3/2,1/2) 2	99	$^3F_2$	82			37	0.006	2.759
(F) 94.41	94.32	94.98	(12) 92.59	(3/2,1/2) 1	89	$^1P_1$	56	$^3P_1$	25	44	0.026	0.743

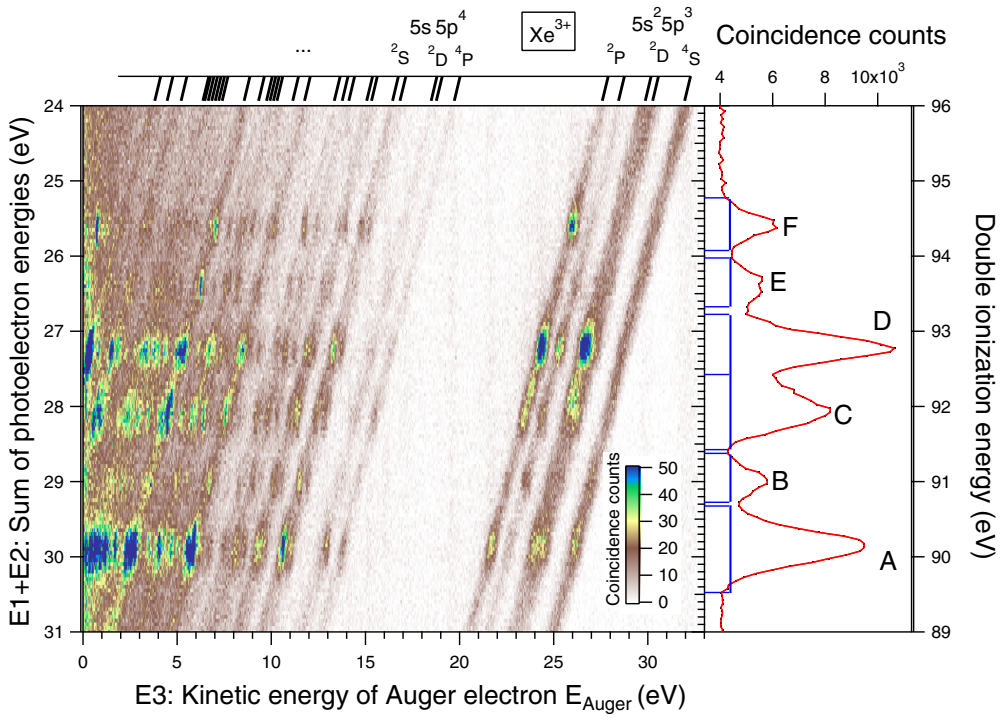

FIG. 4. Experiment with HERMES setup. Core valence double photoionization of neutral Xe atoms at 120-eV photon energy. Left: Coincidence map for events where three electrons have been detected in coincidence. The coincidence map shows the energy correlations between the sum of the kinetic energies of two of them ($E1 + E2$) (y axis) vs the kinetic energy of the third one $E3$ (x axis). The right panel shows the projection of the coincidence map on the y axis, revealing the $Xe^{2+}\,4d^{-1}\,5p^{-1}$ states. The rectangles indicate the peak boundaries selected for the analysis of the Auger spectra in Figs. 6 and 7.

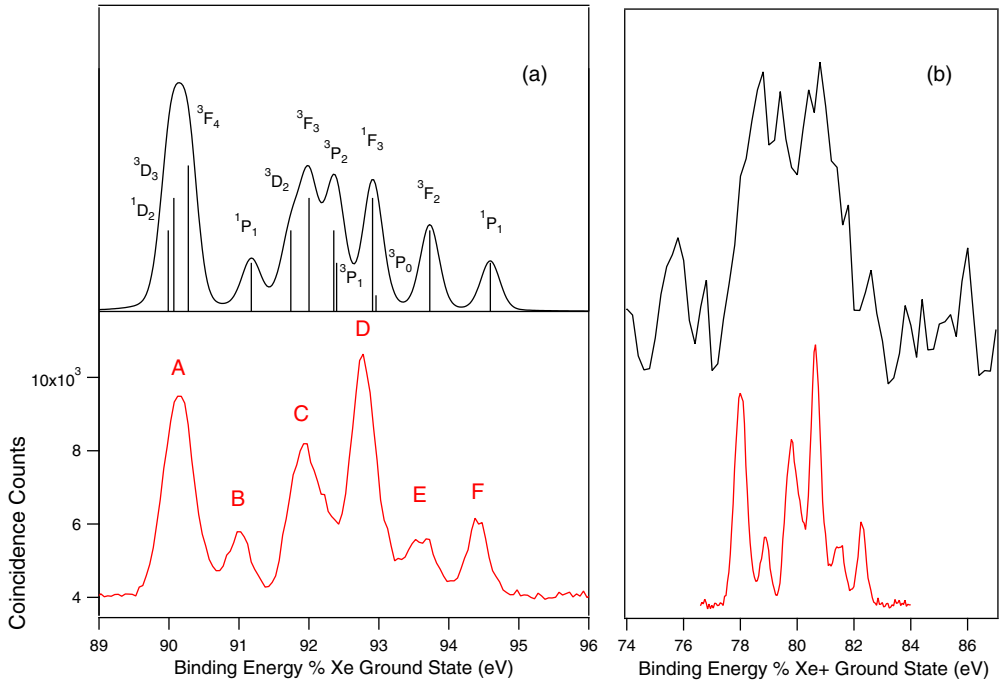

FIG. 5. (a) Bottom (red): Xe^{2+*} ($4d^{-1}\,5p^{-1}$) states observed by core valence double ionization, from Fig. 4 (right). The vertical bars represent the energy positions and intensities obtained from the fit analysis (see text). Top: Our calculations (see Table I for assignment of peaks); intensity is given by statistical populations. Note that the theoretical curves have been shifted by +2 eV to match the positions of the experimental peaks. (b): Comparison between MAIA and HERMES experimental results.

are formed presumably with different relative populations because of the different formation mechanisms, it is possible to compare directly the binding energies obtained by the two methods. The experiment consists in searching for the three-electron coincidence events (e^-_{ph1}, e^-_{ph2}, e^-_{Auger}) associated with reaction (2) from the multi coincidence data set obtained by HERMES. In Fig. 4 we plot energy correlations for such three electron events, presenting them as a function of the sum $E1 + E2$ of the kinetic energies of two electrons from the triplet (y axis) and of the kinetic energy $E3$ of the third electron (x axis). The energy scale ranges in Fig. 4 are selected so that $E1 + E2$ matches the sum of kinetic energies of the two photoelectrons and $E3$ matches the energy of the Auger electron. The two-dimensional plot shows diagonal lines on which intense dots are superimposed, plus a weak background continuum of false coincidences which increases in intensity at low $E3$ values.

Along each diagonal line, the sum of the kinetic energies of the three electrons ($E1 + E2 + E3$) is constant, indicating that these lines correspond to true coincidences associated with the formation of different Xe^{3+} final states, which are labeled above the triple coincidence map in Fig. 4. Apart from the core valence double ionization followed by an Auger decay (2), two other processes can contribute to the intensity of diagonal lines: direct triple ionization which is expected to be weak and unstructured, and double Auger decay of $Xe^+ 4d^{-1}$ states and of their satellites. Double Auger decay of $Xe^+ 4d^{-1}$ holes has been studied by Penent *et al.* [26]; that of the $4d^{-1}$ satellites has not been reported in the literature to the best of our knowledge, but it is expected that they behave similarly to those of the $Kr^+ 3d^{-1}$ satellites studied by Andersson *et al.* [27]. From these studies and from energy considerations, we can deduce that double Auger decay of $Xe^+ 4d^{-1}$ and of the corresponding satellite states will not contribute in the energy range of Fig. 4. The core valence double ionization contribution that we are looking for will increase the intensities at specific "spots" along the diagonal lines when the third electron e^-_3 is the Auger electron. These spots are elongated in the vertical direction because the absolute energy resolution for the low energy $E3$ electrons is better than for the sum of ($E1 + E2$). Since in the present case all Auger electron energies lie within the range covered by the possible energies of the two photoelectrons, the core valence double ionization itself will also contribute to the background intensity along the diagonal lines of Fig. 4. These contributions are caused by the combinations (e^-_1, e^-_2, e^-_3) of the type (e^-_{ph1}, e^-_{Auger}, e^-_{ph2}), i.e., where e^-_3 is a photoelectron and e^-_1 or e^-_2 is the Auger electron; they show for a given Auger energy E_{Auger} the energy sharing between the two photoelectrons. This type of energy sharing is found to be mainly flat and unstructured due to the dominant direct core valence double photoionization process. However, the sharing contains also minor structured contributions of weak cascade processes caused by the formation of highly excited $Xe^+ 4d^{-1} 5p^{-1} nl$ satellite states and their subsequent spin-flip Auger decay to $Xe^{2+} 4d^{-1} 5p^{-1}$ states with the release of a low-energy Auger electron. Such type of energy sharing is not shown here, but it is similar to those observed in the core valence double photoionization paths $1s^{-1}2p^{-1}$ in Ne [7],

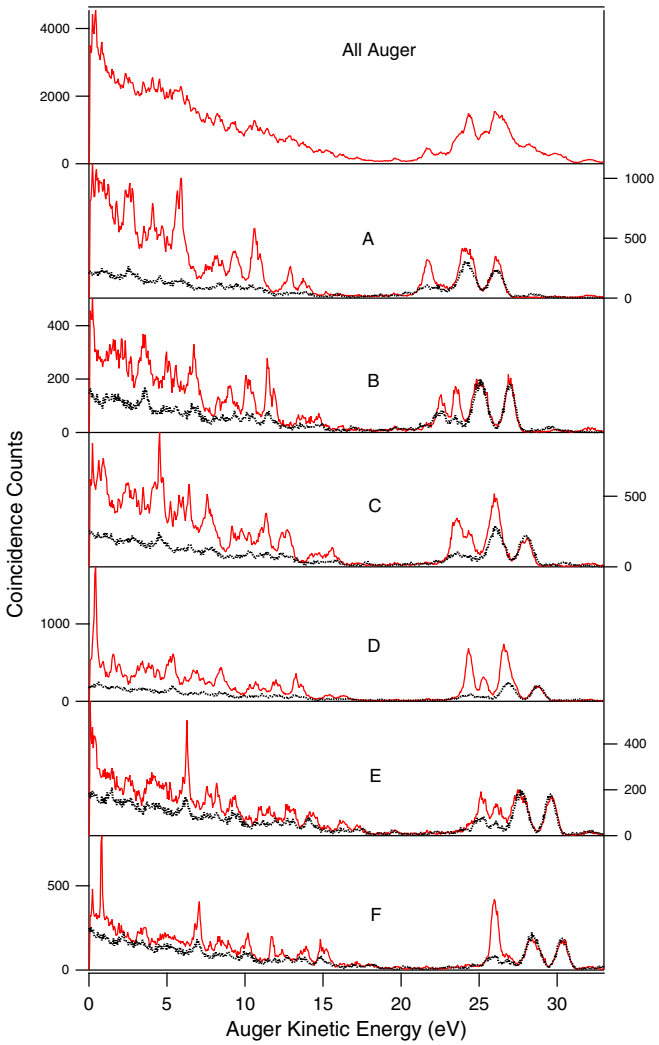

FIG. 6. Experiment with HERMES setup. Auger spectra for the decay of each group of $Xe^{2+} 4d^{-1} 5p^{-1}$ core valence states defined in Figs. 4 and 5. These Auger spectra are deduced from the experiment in Fig. 4, as the intensity along each line associated to the corresponding group of core valence states. The black dotted lines give the estimated background, obtained out of the core valence peak region (see text for further explanation).

$2p^{-1}3p^{-1}$ in Ar [28], $4f^{-1}6s^{-1}$ and $4f^{-1}5d^{-1}$ in Hg [9], or $3d^{-1}4p^{-1}$ in Kr [11].

The spots along the lines in Fig. 4 thus give access to process (2). The horizontal bands formed by the spots trace the different Xe^{2+*} ($4d^{-1} 5p^{-1}$) intermediate states, while the abscissa of the spots along the lines give the kinetic energies for their Auger decays. Integration along the x axis gives the spectrum of the Xe^{2+*} ($4d^{-1} 5p^{-1}$) states which is presented on the right-hand side of Fig. 4. This spectrum is presented by dots in the bottom of Fig. 5(a) and shows six broad peaks. In order to reproduce also the asymmetric shape of peak C it is fitted by seven Voight profiles with a fixed Lorentzian contribution and widths of 70 ± 30 meV, which agrees well with the averaged calculated lifetime broadening reported in

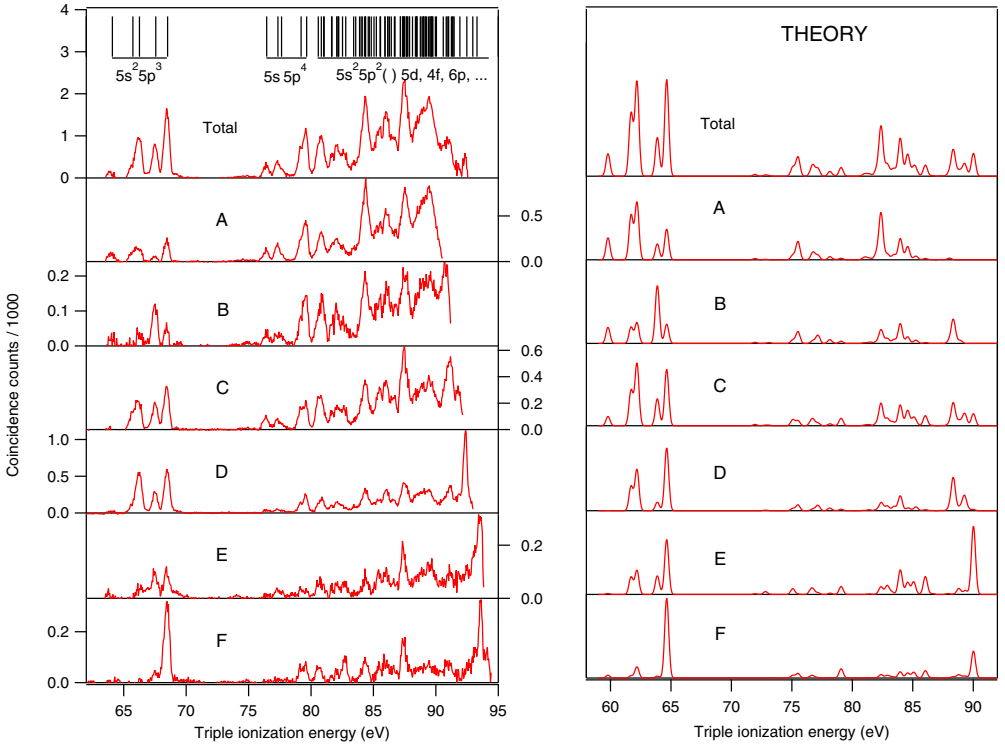

FIG. 7. The Xe^{3+} final-state energy spectra for the Auger decay of the Xe^{2+} $4d^{-1}\,5p^{-1}$ core valence states, represented as a function of the binding energy of the final Xe^{3+} states: experiment with HERMES setup (left) and theory (right). The top panels present the total final-state energy spectra while the panels (A)–(F) show the spectra of the different groups of $4d^{-1}\,5p^{-1}$ states defined in Figs. 4 and 5. The experimental results have been obtained by integration along the diagonal lines in Fig. 4. Contrary to Fig. 6, the background has been subtracted here. The spectra are calibrated using a triple ionization energy of 64.09 eV [26] for the ground state of Xe^{3+}. The vertical bars above the uppermost panels indicate the energy positions and assignments of the Xe^{3+} levels as reported in the NIST tables.

Table I. The Gaussian widths for the two components of peak C, as well as for peaks B, E, and F which are predicted to correspond to a single Xe^{2+*} $(4d^{-1}\,5p^{-1})$ state, amount to 350 ± 30 meV and are mainly caused by the experimental resolution. Larger Gaussian widths were necessary to fit peaks A and D, reflecting the presence of the unresolved components predicted by theory. The resulting experimental binding energies are reported in Table I. They match very well the results deduced from the $4p$ Auger decay of Kivimäki *et al.* [25], but are found ~200–500 meV lower than the values obtained by Bolognesi *et al.* [29] in their threshold-photoelectron coincidence spectra. Our calculated results, shown in the top panel of Fig. 5(a), reproduce well the photoelectron spectrum, enabling the identification of the observed Xe^{2+*} $(4d^{-1}\,5p^{-1})$ states. The calculated binding energies are found to lie ~2 eV below the observed values, which is typical of this kind of *ab initio* calculations. In the present approach the intensities are obtained by simply assuming that individual Xe^{2+*} $(^{S}L_{J})$ states are populated according to their $(2J+1)$ statistical weight. In this way a good overall agreement with the measured spectrum is obtained which possibly reflects the nature of the observed dominant direct double photoionization process. Small differences remain, such as a too low predicted intensity for the D band; it is expected that they can be explained with more accurate *ab initio* calculations, such as those developed by Fritzsche and coworkers for Kr [11] and Hg [9] core valence double ionization. Note that the predicted lifetimes of the Xe^{2+*} $(4d^{-1}\,5p^{-1})$ states vary by a factor 2 and are on average longer than the lifetimes of a single $4d^{-1}$ hole: Jurvansuu *et al.* [15] measured a lifetime broadening of 104 ± 3 meV for the Xe^{+} $(4d^{-1})$ $^{2}D_{3/2}$ state and of 111 ± 3 meV for the $(4d^{-1})$ $^{2}D_{3/2}$ one. This on average longer lifetime can be explained by the main decay processes of the $4d^{-1}$ hole, which is the $N_{4,5}OO$ Auger decay. In case of a $4d^{-1}$ hole in Xe^{2+*} $(4d^{-1}\,5p^{-1})$ there is one $5p$ electron less in the O shell as compared to the Xe^{+} $(4d^{-1})$ state. This reduces the number of possible $N_{4,5}OO$ Auger channels and increases the lifetime. The resolution in the present paper is unfortunately not sufficient to probe lifetime predictions.

Finally we compare in Fig. 5(b) our measurement of the Xe^{2+*} $(4d^{-1}\,5p^{-1})$ states reached by core valence double ionization of the Xe atom, to that of Fig. 3 where they are reached by $4d$ ionization of the Xe^{+} ion. This comparison demonstrates the difficulty of performing photoelectron spectroscopy on ionic targets, but also fully confirms that our determination of the $4d$ photoelectron spectrum from Xe^{+} ions is correct.

2. *Auger decay of the* Xe^{2+} $4d^{-1}\,5p^{-1}$ *states*

From Fig. 4 one can extract the Auger spectrum for each of the six resolved components A to F of Xe^{2+*} $(4d^{-1}\,5p^{-1})$

initial states. These spectra are given by the intensity along each of the corresponding horizontal lines in the three-electron correlation map, and are represented in Fig. 6. The background signal due to the unstructured intensity along the diagonal lines is represented by black curves. It has been estimated from the signal at $E1 + E2$ energies in the 24–25-eV range where no Xe^{2+*} ($4d^{-1}\,5p^{-1}$) states are present. The Auger spectra of the six components A to F are obviously very different. Note that the fastest Auger electron has a kinetic energy around 28 eV, an energy well below the fastest Auger electron energy (36.422 eV) associated with the decay of Xe^+ ($4d^{-1}$) states [20].

In order to understand better the Auger decay path [Fig. 2(b)], we have calculated these Auger spectra following the method described in Sec. III. They are represented in the right panel of Fig. 7 and are plotted, contrary to Fig. 6, as a function of the triple ionization energy, i.e., the binding energy of the final Xe^{3+} states. In this way only five peaks are obtained for the Auger decay to Xe^{3+} ($5s^2\,5p^3$) states, even for Xe^{2+*} bands with unresolved states, such as A. These predictions are compared to the experiment results shown in the left panel of Fig. 7, which have been obtained by integration along the diagonal lines of the two-dimensional plot of Fig. 4 (instead of a simple projection on the x axis, as was done for Fig. 6). Background has been subtracted from the experimental curves in Fig. 7. One observes an excellent agreement between theory and experiment, especially for the Auger decays ending in the lower Xe^{3+} ($5s^2\,5p^3$) states. The strong selectivity of the Auger decay is nicely reproduced; see for instance the decay of the Xe^{2+*} ($^1P_1$) state (F peak) which is found both experimentally and by theory to populate selectively the $^2P_{3/2}$ level of the Xe^{3+} ($5s^2\,5p^3$) states. Figure 7 shows that agreement is less good for the slower Auger electrons associated with the population of the higher-energy Xe^{3+} final states. Two reasons can be invoked: some background may remain in our experimental spectrum and more configurations should be included in the calculations.

V. CONCLUSION

We have measured directly the 4d photoelectron spectrum of Xe^+ ions of both the $^2P_{3/2}$ ground state and the $^2P_{1/2}$ metastable state. Such a measurement is extremely difficult due to the low density of ion beams and was possible only thanks to the availability of an intense synchrotron source such as the PLEIADES beam line, and thanks to the use of electron-ion coincidence techniques. Our results are at variance with the earlier result from Gottwald *et al.* [4], but we validate them by calculations and by a complementary experimental method, namely, the core valence double ionization of the neutral Xe atom. This approach gives detailed access to the spectroscopy of the Xe^{2+*} ($4d^{-1}\,5p^{-1}$) levels which are also populated by inner-shell ionization of Xe^+ ions. Moreover, we studied the Auger decay of the Xe^{2+*} ($4d^{-1}\,5p^{-1}$) levels, which is found to be extremely selective. These results are another example of the power of multielectron coincidence experiments studies of the multiphotoionization of neutral atoms, to retrieve information on the photoionization process of ions, that we illustrated in the case of a $2p$ inner-shell ionization of an Ar^+ ion [8].

ACKNOWLEDGMENTS

The experiment was performed at SOLEIL Synchrotron (France) at the PLEIADES and SEXTANTS beam line, with the approval of the SOLEIL Peer Review Committee (Projects No. 20150198 and No. 20150359). We are grateful to J. Bozek, A. R. Milosavljevic, C. Nicolas, E. Robert, N. Jaouen, and PLEIADES and SEXTANTS teams for help during the measurements, and to SOLEIL staff for stable operation of the storage ring. We are indebted to P. Selles for fruitful discussions. M.A.K. acknowledges the support of the Labex Plas@Par managed by the Agence Nationale de la Recherche, as part of the "Programme d'Investissements d'Avenir" under Reference No. ANR-11-IDEX-0004-02. This work has been financially supported by the Research Council for Natural Sciences and Engineering of the Academy of Finland.

[1] J. M. Bizau, D. Cubaynes, M. Richter, F. J. Wuilleumier, J. Obert, J. C. Putaux, T. J. Morgan, E. Källne, S. Sorensen, and A. Damany, First Observation of Photoelectron Spectra Emitted in the Photoionization of a Singly Charged-ion Beam with Synchrotron Radiation, Phys. Rev. Lett. **67**, 576 (1991).

[2] S. Al Moussalami, J. M. Bizau, B. Rouvellou, D. Cubaynes, L. Journel, F. J. Wuilleumier, J. Obert, J. C. Putaux, T. J. Morgan, and M. Richter, First Angle-Resolved Photoelectron Measurements following Inner-Shell Resonant Excitation in a Singly Charged Ion, Phys. Rev. Lett. **76**, 4496 (1996).

[3] A. Gottwald, S. Anger, J.-M. Bizau, D. Rosenthal, and M. Richter, Inner-shell resonances in metastable Ca^+ ions, Phys. Rev. A **55**, 3941 (1997); A. Gottwald, Ph.D. thesis, Technischen Universität Berlin, 1999.

[4] A. Gottwald, C. Gerth, and M. Richter, 4d Photoionization of Free Singly Charged Xenon Ions, Phys. Rev. Lett. **82**, 2068 (1999).

[5] J. M. Bizau, D. Cubaynes, S. Guilbaud, N. El Eassan, M. M. Al Shorman, E. Bouisset, J. Guigand, O. Moustier, A. Marié, E. Nadal, E. Robert, C. Nicolas, and C. Miron, A merged-beam setup at SOLEIL dedicated to photoelectron–photoion coincidence studies on ionic species, J. Electron Spectrosc. Relat. Phenom. **210**, 5 (2016).

[6] J.-M. Bizau, D. Cubaynes, S. Guilbaud, F. Penent, P. Lablanquie, L. Andric, J. Palaudoux, M. M. Al Shorman, and C. Blancard, Photoelectron Spectroscopy of Ions: Study of the Auger Decay of the $4d \rightarrow nf$ ($n = 4,5$) Resonances in Xe^{5+} Ion, Phys. Rev. Lett. **116**, 103001 (2016).

[7] Y. Hikosaka, T. Aoto, P. Lablanquie, F. Penent, E. Shigemasa, and K. Ito, Experimental Investigation of Core-Valence Double Photoionization, Phys. Rev. Lett. **97**, 053003 (2006).

[8] S.-M. Huttula, P. Lablanquie, L. Andric, J. Palaudoux, M. Huttula, S. Sheinerman, E. Shigemasa, Y. Hikosaka, K. Ito, and F. Penent, Decay of a $2p$ Inner-Shell Hole in an Ar^+ Ion, Phys. Rev. Lett. **110**, 113002 (2013).

[9] M. Huttula, S.-M. Huttula, S. Fritzsche, P. Lablanquie, F. Penent, J. Palaudoux, and L. Andric, Core-valence double photoionization of atomic mercury, Phys. Rev. A **89**, 013411 (2014).

[10] S.-M. Huttula, J. Soronen, M. Huttula, F. Penent, J. Palaudoux, L. Andric, and P. Lablanquie, Auger decay of core valence

double photoionized states in atomic mercury, J. Phys. B **48**, 115001 (2015).

[11] E. Andersson, P. Linusson, S. Fritzsche, L. Hedin, J. H. D. Eland, L. Karlsson, J.-E. Rubensson, and R. Feifel, Formation of Kr^{3+} via core-valence doubly ionized intermediate states, Phys. Rev. A **85**, 032502 (2012).

[12] B. Rouvellou, J. M. Bizau, D. Cubaynes, L. Journel, and S. Al Moussalami, and F. J. Wuilleumier, A dedicated electron spectrometer for photoionization studies of atomic ions with synchrotron radiation, J. Electron Spectrosc. Relat. Phenom. **76**, 237 (1995).

[13] S. Jullien, J. Lemaire, S. Fenistein, M. Heninger, G. Mauclaire, and R. Marx, Radiative lifetimes of Xe^+ and Kr^+ in their $^2P_{12}$ spin-orbit states, Chem. Phys. Lett. **212**, 340 (1993).

[14] P. Andersen, T. Andersen, F. Folkmann, V. K. Ivanov, H. Kjeldsen, and J. B. West, Absolute cross sections for the photoionization of $4d$ electrons in Xe^+ and Xe^{2+} ions, J. Phys. B **34**, 2009 (2001).

[15] M. Jurvansuu, A. Kivimäki, and S. Aksela, Inherent lifetime widths of Ar $2p^{-1}$, Kr $3d^{-1}$, Xe $3d^{-1}$, and Xe $4d^{-1}$ states, Phys. Rev. A **64**, 012502 (2001).

[16] M. Sacchi, N. Jaouen, H. Popescu, R. Gaudemer, J. M. Tonnerre, S. G. Chiuzbaian, C. F. Hague, A. Delmotte, J. M. Dubuisson, G. Cauchon, B. Lagarde, and F. Polack, The SEXTANTS beamline at SOLEIL: A new facility for elastic, inelastic and coherent scattering of soft X-rays, J. Phys.: Conf. Ser. **425**, 072018 (2013).

[17] J. Palaudoux, S. Sheinerman, J. Soronen, S.-M. Huttula, M. Huttula, K. Jänkälä, L. Andric, K. Ito, P. Lablanquie, F. Penent, J.-M. Bizau, S. Guilbaud, and D. Cubaynes, Valence Auger decay following $3s$ photoionization in potassium, Phys. Rev. A **92**, 012510 (2015).

[18] J. H. D. Eland, O. Vieuxmaire, T. Kinugawa, P. Lablanquie, R. I. Hall, and F. Penent, Complete Two-Electron Spectra in Double Photoionization: The Rare Gases Ar, Kr, and Xe, Phys. Rev. Lett. **90**, 053003 (2003).

[19] K. Ito, F. Penent, Y. Hikosaka, E. Shigemasa, I. H. Suzuki, J. H. D. Eland, and P. Lablanquie, Application of a simple asynchronous mechanical light chopper to multielectron coincidence spectroscopy, Rev. Sci. Instrum. **80**, 123101 (2009).

[20] T. Carroll, J. Bozek, E. Kukk, V. Myrseth, L. Sæthre, T. Thomas, and K. Wiesner, Xenon $N_{4,5}OO$ Auger spectrum—a useful calibration source, J. Electron Spectrosc. Relat. Phenom. **125**, 127 (2002).

[21] P. Jönsson, X. He, C. Froese Fischer, and I. P. Grant, The grasp2K relativistic atomic structure package, Comput. Phys. Commun. **177**, 597 (2007).

[22] K. G. Dyall, I. P. Grant, C. T. Johnson, F. A. Parpia, and E. P. Plummer, GRASP: A general-purpose relativistic atomic structure program, Comput. Phys. Commun. **55**, 425 (1989).

[23] S. Fritzsche, The Ratip program for relativistic calculations of atomic transition, ionization and recombination properties, Comput. Phys. Commun. **183**, 1525 (2012).

[24] G. Gaigalas, T. Zalandauskas, and S. Fritzsche, Spectroscopic LSJ notation for atomic levels obtained from relativistic calculations, Comput. Phys. Commun. **157**, 239 (2004).

[25] A. Kivimäki, H. Aksela, J. Jauhiainen, M. Kivilompolo, E. Nõmmiste, and S. Aksela, Interpretation of the $N_{2,3}N_{4,5}O_{2,3}$ Coster-Kronig spectrum of xenon, J. Electron Spectrosc. Relat. Phenom. **93**, 89 (1998).

[26] F. Penent, J. Palaudoux, P. Lablanquie, L. Andric, R. Feifel, and J. H. D. Eland, Multielectron Spectroscopy: The Xenon $4d$ Hole Double Auger Decay, Phys. Rev. Lett. **95**, 083002 (2005).

[27] E. Andersson, S. Fritzsche, P. Linusson, L. Hedin, J. H. D. Eland, J.-E. Rubensson, L. Karlsson, and R. Feifel, Multielectron coincidence study of the double Auger decay of $3d$ -ionized krypton, Phys. Rev. A **82**, 043418 (2010).

[28] M. Nakano, Y. Hikosaka, P. Lablanquie, F. Penent, S.-M. Huttula, I. H. Suzuki, K. Soejima, N. Kouchi, and K. Ito, Auger decay of Ar $2p$ satellite states studied with a multielectron coincidence method, Phys. Rev. A **85**, 043405 (2012).

[29] P. Bolognesi, L. Avaldi, M. C. A. Lopes, G. Dawber, G. C. King, M. A. MacDonald, C. Villani, and F. Tarantelli, Direct observation of the Kr $(3d^{-1}4p^{-1})$ and Xe $(4d^{-1}5p^{-1})$ doubly charged ion states by threshold-photoelectron coincidence spectroscopy, Phys. Rev. A **64**, 012701 (2001).